*energies*

MDPI

*Article*

# Laser Modified Glass for High-Performance Photovoltaic Module

**Olgierd Jeremiasz [1,2], Paweł Nowak [2], Franciszek Szendera [2], Piotr Sobik [2], Grażyna Kulesza-Matlak [1], Paweł Karasiński [3], Wojciech Filipowski [4] and Kazimierz Drabczyk [1,*]**

[1] Institute of Metallurgy and Materials Science, Polish Academy of Sciences, ul. Reymonta 25, 30-059 Kraków, Poland
[2] Helioenergia Sp. z o.o. ul., Rybnicka 68, 44-238 Czerwionka-Leszczyny, Poland
[3] Department of Optoelectronics, Silesian University of Technology, ul. Krzywoustego 2, 44-100 Gliwice, Poland
[4] Faculty of Automatic Control, Electronics and Computer Science, Silesian University of Technology, ul. Akademicka 16, 44-100 Gliwice, Poland
* Correspondence: kazimierz.drabczyk@wp.pl

**Abstract:** The solar module output power is the power generated by all individual cells in their specific electrical circuit configuration, multiplied by the cell-to-module power ratio. The cell-to-module power ratio thus reflects the sum of the losses and gains produced by the structure of the module. The biggest process change in module design during the last few years was the introduction of half cells. Another important trend is the use of bifacial cells to build bifacial modules. These two trends increase parts of the module that correspond to the intercell gaps, and the light does not meet the cell in its path. This part of the radiation is therefore not used efficiently. Scientific efforts focus on the texturing surface of covering glass and cells, and the introduction of narrower ribbons and encapsulation materials with improved UV performance, etc. The concept of a diffusor that actively redirects light from the intercell space into the cell was proposed in the past, in the form of a micro-structured prismatic film, but this is not applicable for bifacial modules. The conclusion is that losses caused by the incidence of light on the areas of the photovoltaic panel not covered with solar cells yet are to be explored further. A sawtooth-shaped reflecting diffusor placed between cells is proposed. This article addresses the issue in a novel way, primarily because the theoretical range of the optimum sawtooth profile is defined. In the experimental part of the study, the possibility of producing such a profile directly on glass using a $CO_2$ laser is demonstrated. The theoretical model enables discrimination between advantageous and disadvantageous sawtooth profiles. As a proof of concept, minimodules based on the optimum parameters were built and tested for their electrical performance. The result confirms that the proposed sawtooth-shaped reflecting diffusor placed between cells creates cell-to-module power gain. The proposed laser technology can be incorporated into existing production lines, and can increase the output of any photovoltaic technology, including and beyond silicon.

**Keywords:** photovoltaic; $CO_2$ laser; float glass; engraving; cell-to-module power ratio

check for updates

**Citation:** Jeremiasz, O.; Nowak, P.; Szendera, F.; Sobik, P.; Kulesza-Matlak, G.; Karasiński, P.; Filipowski, W.; Drabczyk, K. Laser Modified Glass for High-Performance Photovoltaic Module. *Energies* **2022**, *15*, 6742. https://doi.org/10.3390/en15186742

Academic Editor: Alessandro Cannavale

Received: 22 July 2022
Accepted: 9 September 2022
Published: 15 September 2022

**Publisher's Note:** MDPI stays neutral with regard to jurisdictional claims in published maps and institutional affiliations.

**Copyright:** © 2022 by the authors. Licensee MDPI, Basel, Switzerland. This article is an open access article distributed under the terms and conditions of the Creative Commons Attribution (CC BY) license (https://creativecommons.org/licenses/by/4.0/).

## 1. Introduction

Energy demand is growing globally, but primary energy sources like fossil fuels are gradually depleting. Fossil fuels also affect air quality and public health by emitting greenhouse gases like $CO_2$ and other air pollutants. Based on the current economic growth figures, the world's energy needs will almost double by 2100. Photovoltaics is considered to be the most promising solution for meeting global energy needs, because solar energy is the safest, clean and abundant energy source for future renewable and sustainable energy technologies.

Silicon-based technology is mainstream photovoltaics, and will remain dominant on the market in the coming years [1,2]. A typical photovoltaics module is made of

a glass-backsheet configuration, and laminated with EVA copolymer-based film. The output power of a solar module is the power generated by all the individual cells in their specific electrical circuit configuration, multiplied by the cell-to-module (CTM) power ratio. The CTM ratio is determined by interacting the optical losses and gains, as well as the electrical losses. Higher efficiency and output power at the module level can be achieved by using novel ideas in module technology. Several studies have investigated the role of backsheet reflectance and cell spacing on CTM [3–6]. The growing market share of bifacial cells [2] turned arrangements for PV modules into glass–clear backsheet or glass–glass. The reflecting backsheet is then no longer present. Monofacial modules with bifacial cells are also considered, and are present on the market [2,6]. A significant trend is cell cut technology. Instead of a full cell, half cell, third cell, or quarter cell are used. Half cell technology is becoming dominant [2], increasing the cell spacing area and contributing to efficiency loss in the case of bifacial modules [7,8]. In the case of the parts of the module that correspond to the intercell gaps, the light does not meet the cell in its path. This part of the radiation is therefore not used efficiently. The major advantage of cut cell technology is reduced electrical loss [9]. An interesting way of reducing CTM loss is a shingled structure [10]. These modules are a successful solution for increasing the active surface module and its CTM. The downside of this technology is the need to use additional PV cell processing. Other directions looking for the improvement of CTM are solutions that increase efficiency through the better cooling of PV modules, e.g., via the use of heat sinks, or creating hybrid photovoltaic/thermal systems [11].

Systematic studies are carried out to address CTM in general. Module gains and losses are described and modeled [12–16]. A specific group of solutions focuses on light trapping in solar modules. It is mainly achieved by the texturization of the cover glass surface [17–22] and texturizing cells [23,24]. Both are used to lower the reflectance, so that more light can reach the cells. In the context of texturization, laser technologies are considered [25] in parallel with chemical etching and mechanical treatment.

Light redirecting within the module was addressed by the industry, and sawtooth micro-structured films were proposed and patented [26,27]. The described solution was not introduced into the market, probably because of the cost/effect ratio. A specific feature of the PV industry is the measurement of PV assets volume in Watts-peak (Wp), and quoting PV assets in currency per Wp. This reflects the high competitiveness of the PV industry and the importance of the market embodiment of solutions that are then implemented in the industry. There is a race to increase the efficiency of the photovoltaic conversion, and the scope of losses caused by the incidence of light on the areas of the photovoltaic panel not covered with solar cells yet is to be explored further. In the context of the colossal increase in energy prices, the struggle for every fraction of efficiency is crucial.

The choice of laser technology is justified because it is industry proven and efficient. Laser technologies were studied in the context of glass machining [28–31]. Mechanical methods are still dominating the industry, but laser-based techniques develop and enter the market very quickly. Different lasers are being used for laser drilling and scribing of glass. Laser treatment provides high selectivity and precision, which is necessary.

The concept presented here is mainly dedicated to bifacial modules with bifacial cut cells being the most efficient type of module available. To compensate for the increase of intercell space and the lack of reflecting backsheet, the following paper presents the possibility of using a specific glass geometry in the spaces between cells to increase the CTM coefficient. Glass with such a modification can be used to obtain highly efficient PV modules based on any PV cell technology, including and beyond silicon.

## 2. Materials and Methods

In the proposed solution, the diffuser in the photovoltaic module is engraved in inactive parts of the module, i.e., in the spaces between the cells, on the margins, and above the busbars. $CO_2$ laser radiation interacts with float, soda-lime glass making it possible to engrave and texturize the surface. The diffuser is made as a series of prismatic (triangular

and sawtooth) grooves cut into the glass, which is then covered with a light-reflecting material. The graphic interpretation of this concept is shown in Figure 1.

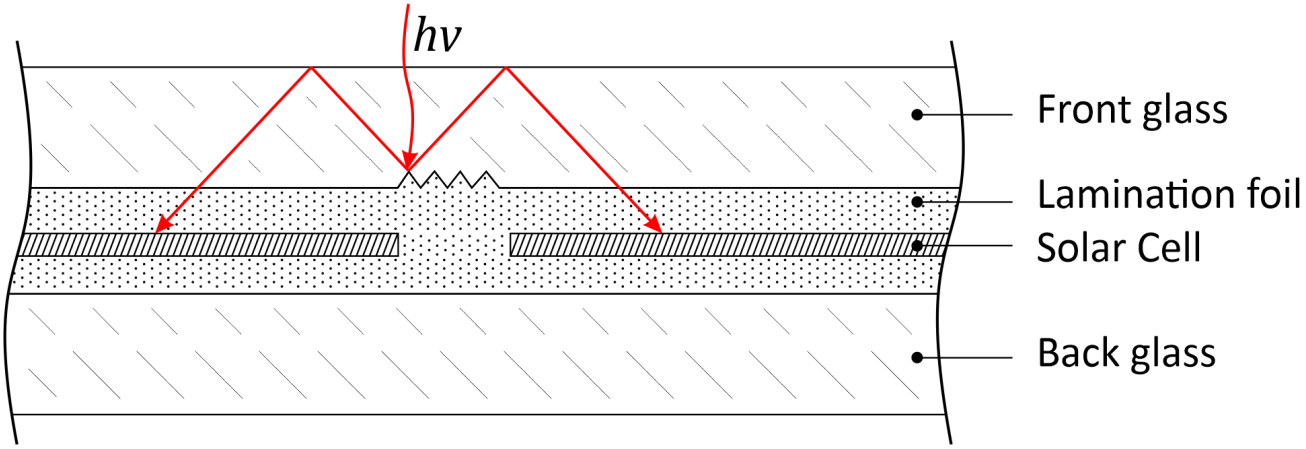


**Figure 1.** Model of the module with a diffuser placed in the inactive (intercell) space of the module.

The system under consideration applies to both single- and double-sided (bifacial) cells. As the analysis of the phenomenon escapes unambiguous assessment, it is difficult to determine what angle of groove opening is optimal for a wide range of angles of incidence. Therefore, an analytical model of the solution was developed.

The model of a single groove is described in Figure 2. The model analyzes the space of a single groove in the form of an isosceles triangle with the opening angle α (pitch angle). The α angle is the primary focus of optimization. The triangle has two reflective planes, no. 1 and no. 2; and plane no. 3, through which the light enters the groove and leaves it after at least one or more reflections. The glass thickness was hypothetically reduced to 0—plane 3 is the surface of the glass.

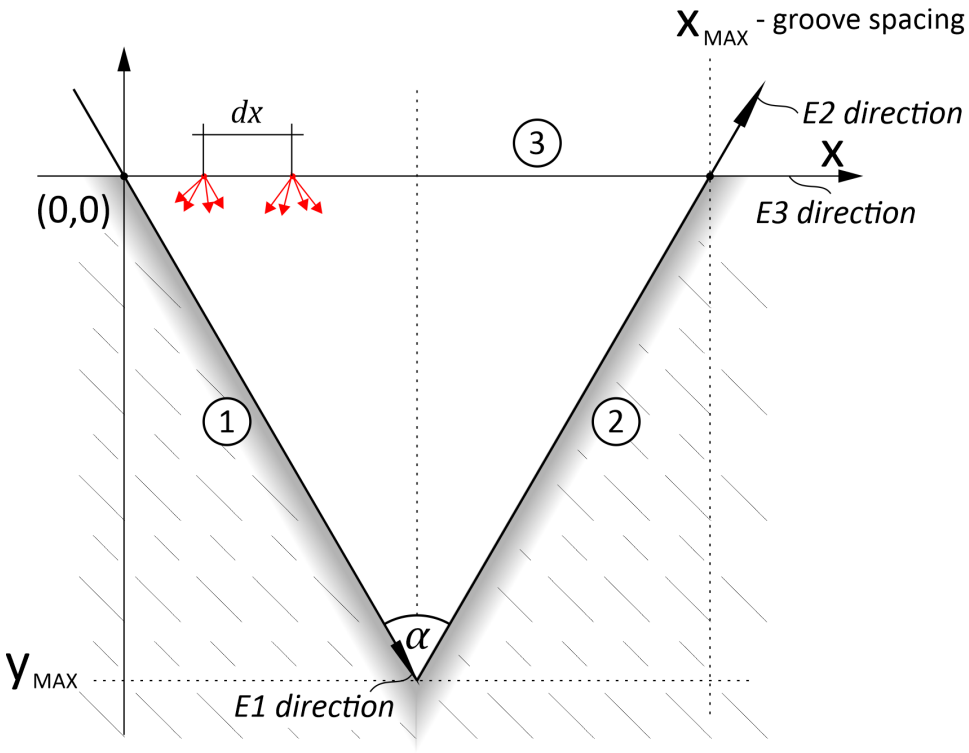


**Figure 2.** Model of the groove used for modeling. 1, 2 reflecting planes, 3—entry/escape plane.

The geometry of the system has been described in the form of vector parameters—i.e., for each element, its starting point cartesian coordinates [$X_1$, $Y_1$], [$X_2$, $Y_2$] and the angle of propagation determined in the full angle system (from 1 to 360°) clockwise; HDG1, HDG2. Refer to Figure 3.

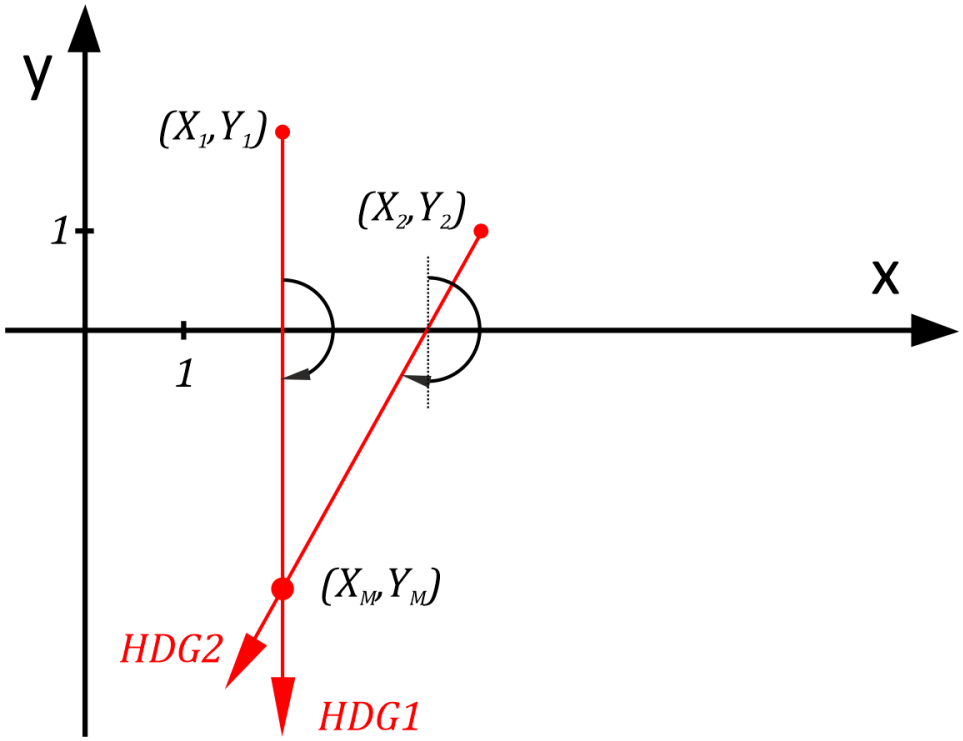


**Figure 3.** Geometry of ray tracing and determination of intersection coordinates using vectors.

The same rule applies to the description of the fixed elements of the diffuser, as well as the ray propagation. Such a definition is favorable in this analysis. In the case of an intersection (meeting) of two rays, the cross-sectional coordinates [$X_m$, $Y_m$] are calculated, and when a reflection takes place—a new propagation angle is calculated.

Determination of intersection coordinates:

Taking $M_1$ = tan (HDG1), $M_2$ = tan (HDG2);

Conditions for intersection:

$X_1 + M_1(Y_m - Y_1) = X_2 + M_2(Y_m - Y_2)$

$X_1 + M_1Y_m - M_1Y_1 = X_2 + M_2Y_m - M_2Y_2$

Solving the above for $X_m$, $Y_m$:

$$X_m = \frac{Y_2 - Y_1 - \frac{X_2}{M_2} + \frac{X_1}{M_1}}{\left(\frac{1}{M_1} - \frac{1}{M_2}\right)}$$

$$Y_m = \frac{X_2 - X_1 - M_2Y_2 + M_1Y_1}{(M_1 - M_2)}$$

The next ray has a starting point at the intersection point [$X_m$, $Y_m$] and a new propagation direction. The simulation ends when the ray escapes the triangle through plane no. 3 (see Figure 4). The angle of escape is checked. For angles outside of the total internal reflection for glass, the ray is classified as non-contributing (value 0). Otherwise, it is added to the number of rays that have a supporting effect. Integration is done along plane no. 3 (see Figure 4) as starting points and the entire incoming ray angle range.

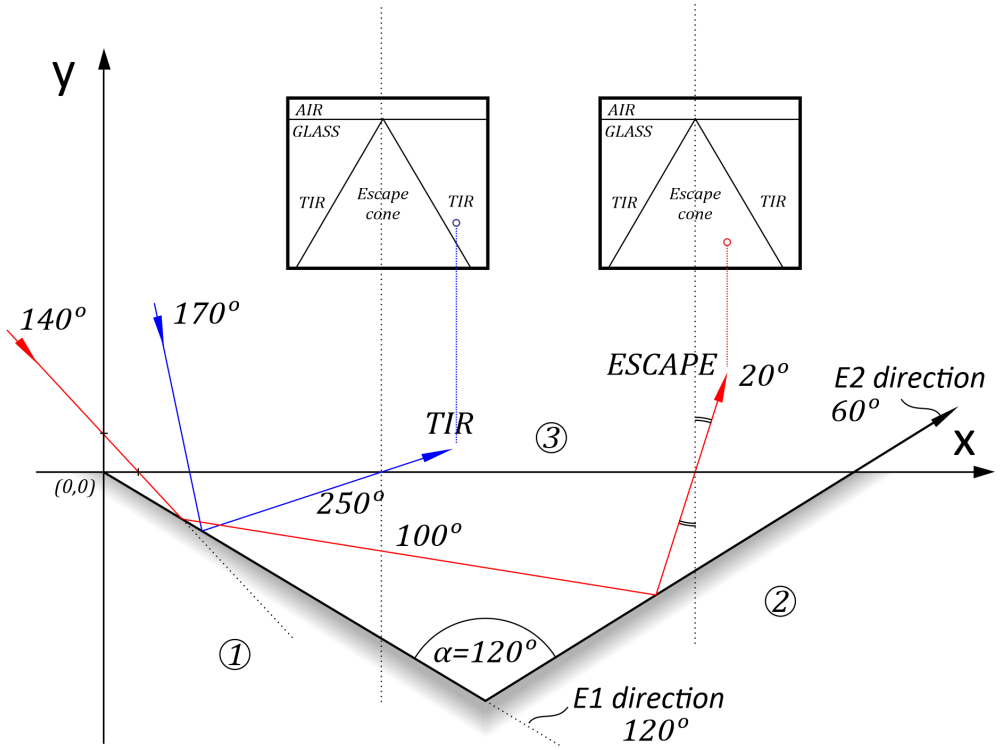


**Figure 4.** Illustration for ray tracing simulation—example for pitch angle 120°. 1, 2 reflecting planes, 3—entry/escape plane.

## 3. Results and Discussion

The above procedure was implemented with Visual Basic for the application code. Efficiency is here defined as the ratio of power successfully redirected from the intercell gap into the solar cell as a portion of the total incoming energy. The index of refraction of the float glass was set to 1.5.

Ray tracing simulations results (Figure 5), clearly show that the optimum angle to achieve is from 122° to 132°. An important finding is that it is also possible to achieve zero percent efficiency; therefore certain angles are to be strictly avoided.

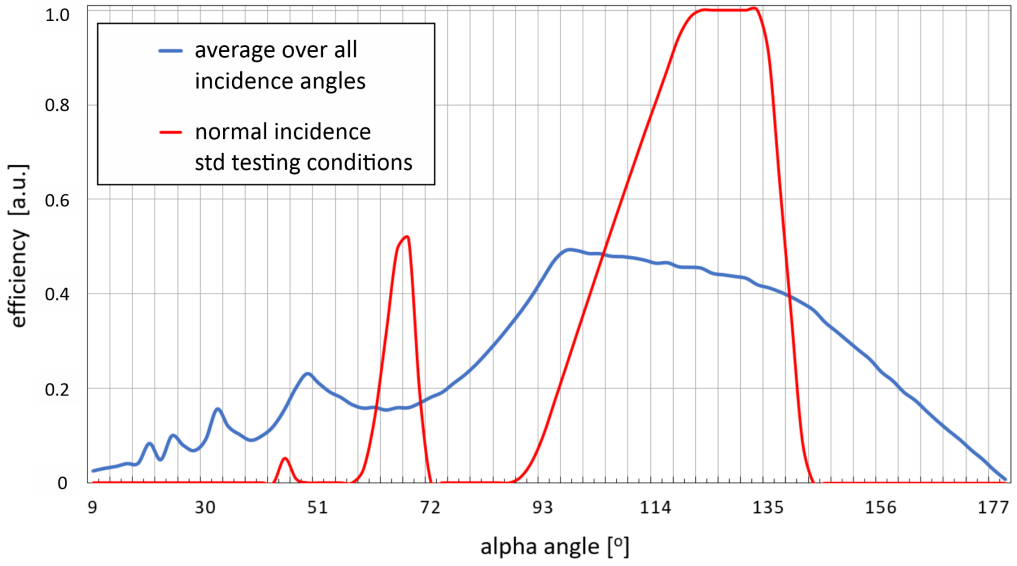


**Figure 5.** Ray tracing simulation results.

An experimental check of the possibility of achieving grooves that are close to the required geometry was performed. $CO_2$ laser and CW mode with a maximum power of 100 W with a X-Y scan stage was used. Trials included focal length (F) 38.1 mm, 50.8 mm, and 127 mm, power (P) from 10 to 90 W, scan speeds (S) from 20 to 600 mm/s, and some experiments performed with water submersion and air assistance. A digital profilometer Keyence VHX was used to measure groove geometry.

CW mode $CO_2$ 10.6 µm laser beam interaction with soda-lime float glass was observed and studied. Glass is a dielectric, amorphous material—considered to be a liquid, and changing viscosity of several orders of magnitude in the function of temperature. The 10.6 µm radiation penetrated glass up to ~40 µm. Float glass contains a significant amount of dissolved gases—0.2 mL per 1 g of glass. According to [32], the typical gas composition is 50% $H_2O$, 33% $SO_2$, 12% $O_2$, and 3% $CO_2$. This is the reason for the visible, observable effects of laser beam interaction with the glass. See Figure 6.

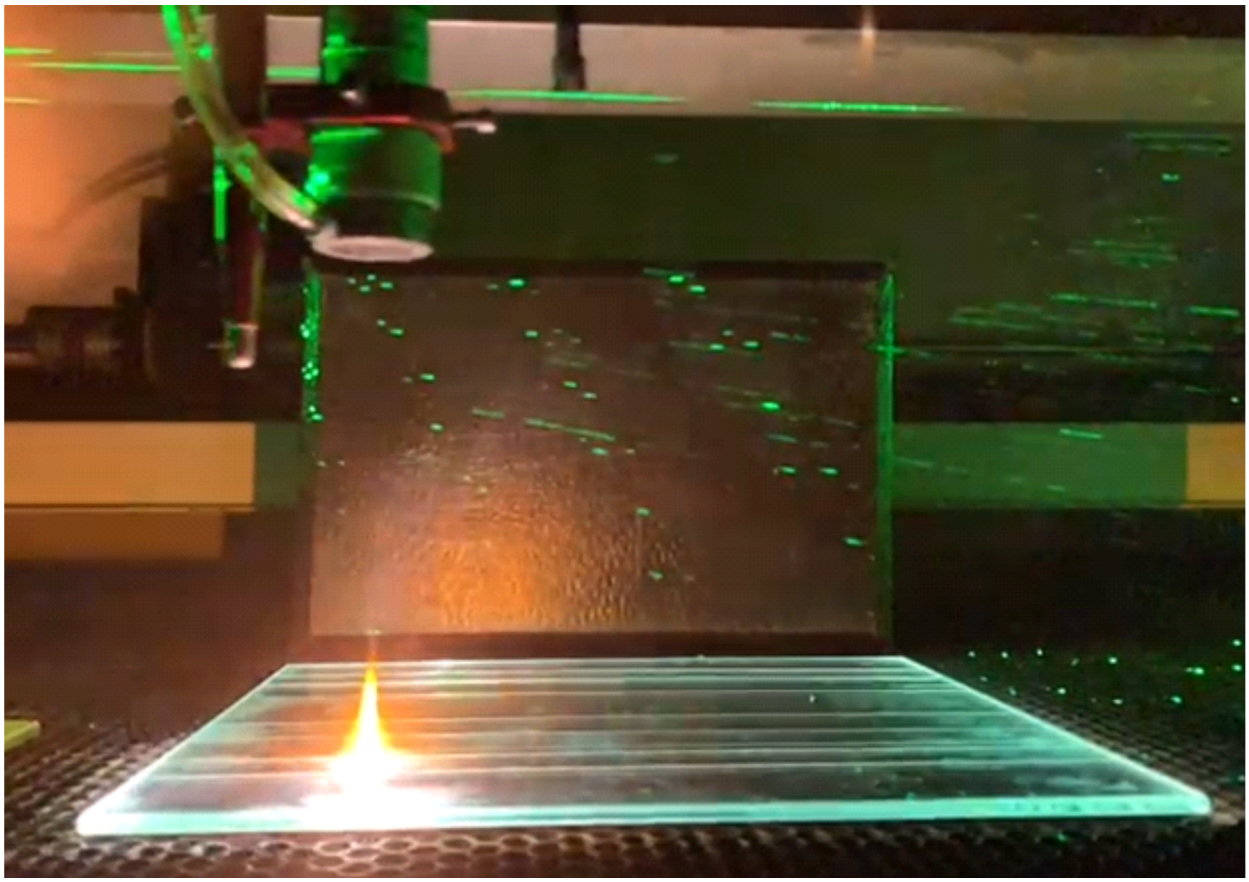

**Figure 6.** Visible effects of CW $CO_2$ laser interaction with soda-lime glass. F = 127 mm. Air assistance protects laser optics and do not influence heat zone.

The following physics of glass–laser interaction is assumed: Glass is heated, and part of the glass is "melted" and ejected with the support of gas evaporation. The heat zone in glass is affected by the expansion and compression of glass, which creates stress, and then leads to cracking. The cracking plane is assumed to be parallel to isotherms due to laser-glass heating [32,33]. A significant glass deposit remains in the groove and has to be removed mechanically. The groove before mechanical removal of the cracked deposit is shown in Figure 7.

Water immersion and air assistance create instabilities, leading to a non-uniform groove shape. Water absorbs 10.6 µm radiation efficiently, and this leads to a non-uniform groove shaped distribution. See Figure 8. The same effect is observed when air assistance is applied in correlation with a short focal length. On the contrary, stable process conditions

with zero air and zero water submersion create a deposit of ejected glass on the laser focusing optics. In the case of a short distance between an object and a focusing lens, the deposit quickly leads to an instability of parameters and lens damage.

A uniform profile in glass is to be achieved only under a stable environment in the processing area (heat zone). Air assistance is allowed only if it does not affect the heating zone—i.e., if the focal length is long enough. Different laser power settings and scan speeds create U- and V-shaped grooves with different pitch angles. After laser treatment, the grooves are mechanically cleaned and the surface is zinc metalized to be subject to inspection using an optical and digital profilometer, Keyence VHX.

The same fluence (laser power divided by scan speed) does not lead to the same shape and size of the groove. A parallel increase of power and scan speed leads to groove narrowing. See Figure 9.

A similar effect is achieved when the scan speed alone is increased while the power remains constant. In case of scan speed increases under constant power, the grooves become more shallow and the pitch angle increases. See Figures 10 and 11. An increase of focal length (F) while the other parameters remain constant leads to a widening of the groove and a transition from a V-shaped to U-shaped profile. See Figure 12.

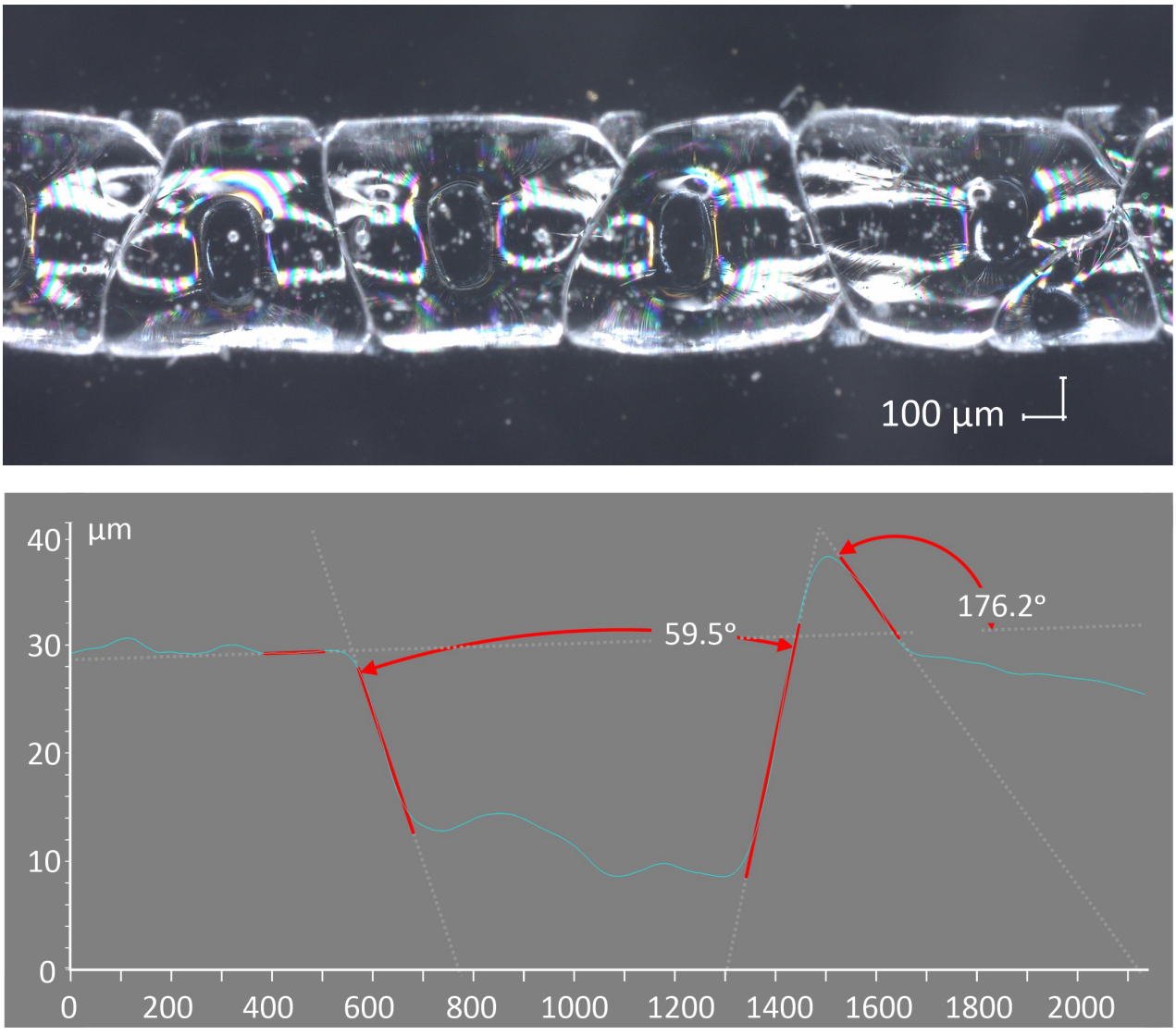


**Figure 7.** Groove before mechanical removal of cracked deposit. (**Top**): Microscope view of groove. (**Bottom**): Cross-sectional profile.

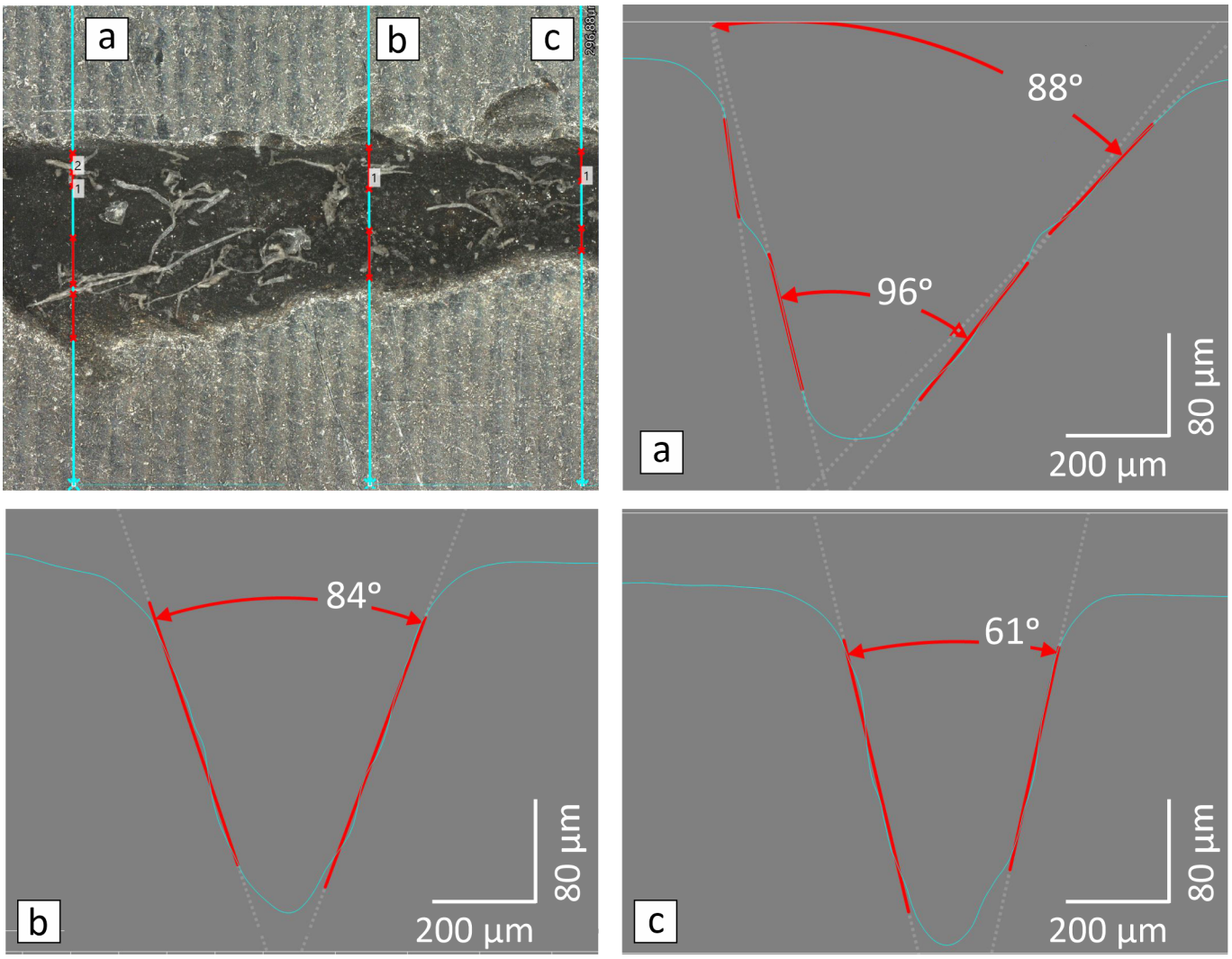


**Figure 8.** Effect of air assistance—significant non-uniformities in groove profile (**a**–**c** are sectional lines).

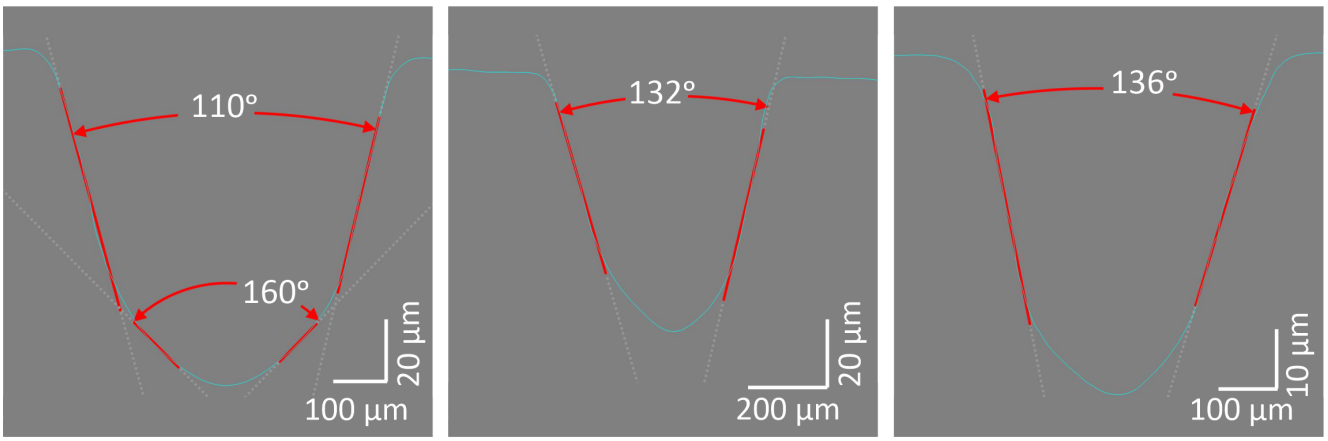


**Figure 9.** Grooves made with same fluence, F = 127 mm. (**left**): P = 30 W, S = 140 mm/s; (**center**): P = 60 W, S = 280 mm/s; (**right**): P = 90 W, S = 520 mm/s.

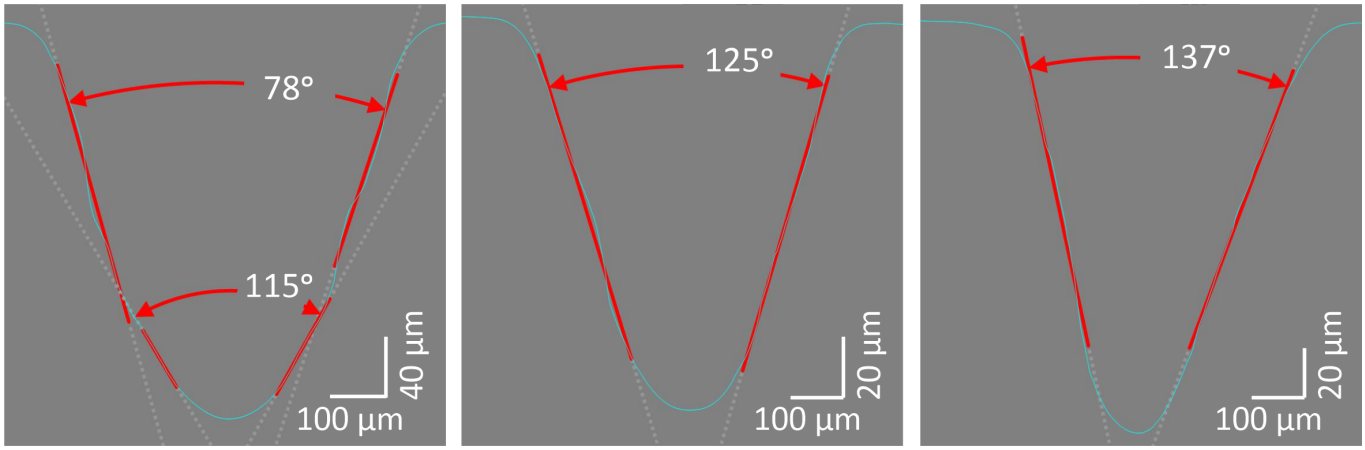


**Figure 10.** Effect of scan speed: F = 38.1 mm, P = 30 W; (**left**): S = 50 mm/s; (**center**): S = 150 mm/s; (**right**): S = 250 mm/s.

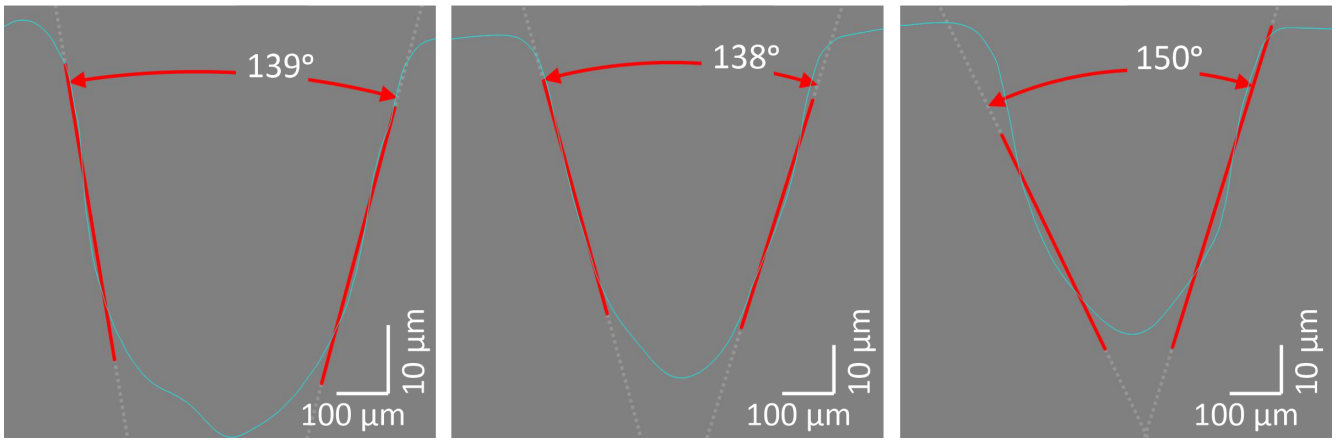


**Figure 11.** Effect of scan speed: F = 127 mm, P = 60 W; (**left**): S = 20 mm/s; (**center**): S = 300 mm/s; (**right**): S = 600 mm/s.

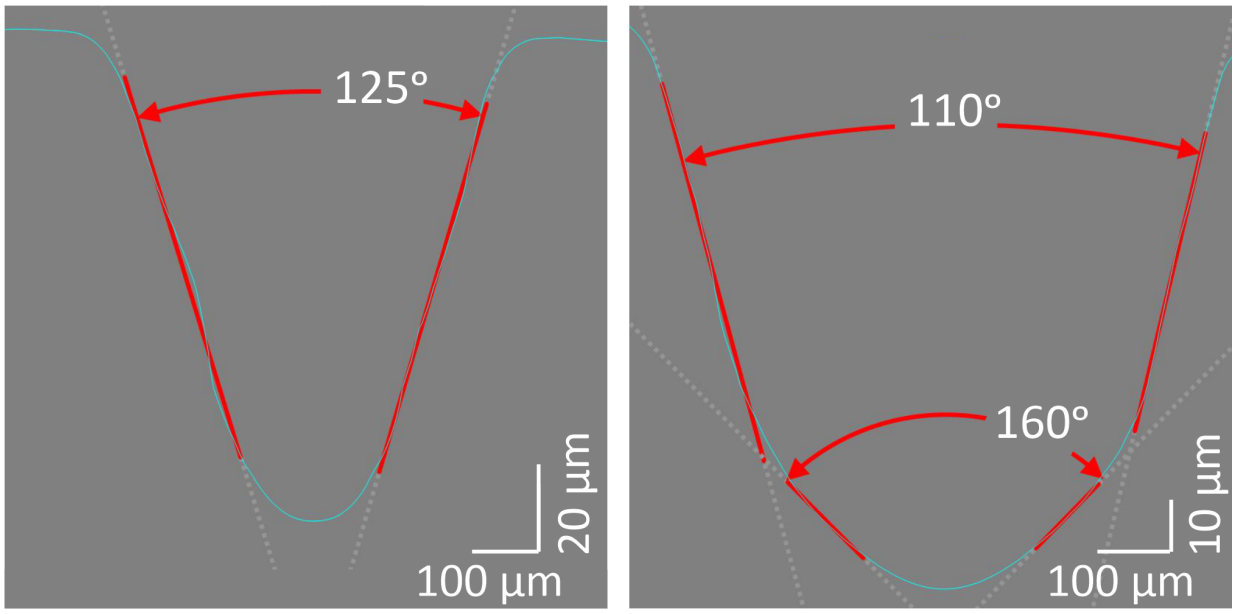


**Figure 12.** Focal length effect: P = 30 W, S = 140 mm/s; (**left**): F = 38.1 mm; (**right**): F = 127 mm.

Grooves that were close in parameters to these compiled from theory are achieved at parameters shown in Figure 13 (left). It shall be noted that it is also possible to make zero percent efficient grooving with a change in laser parameters. Under stable parameters in the heating zone, uniform grooves are achieved. See Figure 13.

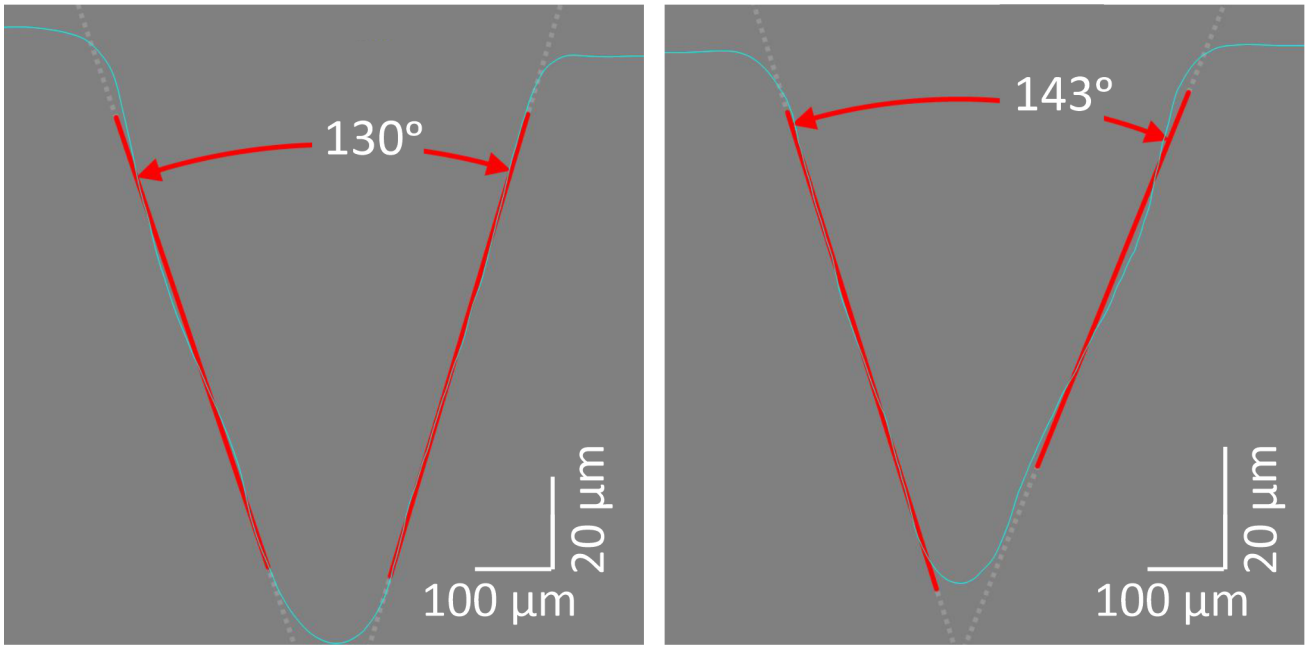


**Figure 13.** Example of V-shaped grooves. F = 38.1 mm, P = 25 W. (**left**): S = 120 mm/s desired pitch angle; (**right**): S = 60 mm/s undesired pitch angle.

Most desired V-shaped grooves are achieved in a power range of 20–30 W and a scan speed of 80–140 mm/s with a short focal length. Longer focal lengths lead to more U-shaped profiles. This undesired effect can be partly compensated by increasing the power and the scan speed. A short focal length means a short distance between the focusing optics and the heat zone, leading to a situation where blowing air is disturbing the heat zone. This leads to an non-uniform groove shape.

A favorable radius at the tip of the groove is achieved in all cases, which ensures a lack of stress concentration around the tip. All tests were performed on regular flat samples of tempered, soda-lime glass. No glass breaking was observed. The groove depth was in the range of 100 µm, which was significantly below the compression layer thickness created by tempering. Changes in mechanical parameters of glass are to be further studied, and their influence on PV module mechanical performance is to be evaluated.

As a proof of concept, two pairs of PV minimodules sized 200 × 200 mm were prepared. There is one reference and one module with laser grooving modification in each pair. For each pair, two pieces of monocrystalline silicone bifacial cells of size 182 mm with 10 busbars with 22.4% efficiency were laser cut into halves and arranged into modules according to the self-compensating scheme explained in Figure 14. Such a procedure enables a direct comparison of efficiency between the modules. Cells were stringed with a 4 mm gap and laminated with PVB foil between 3 mm thick soda-lime tempered float glasses.

Reference modules remained untreated. Modified modules were laser-treated using parameters obtained during the study: F = 50.8 mm, P = 25 W, V = 75 mm/s. Multiple grooves were formed using 550 µm groove-to-groove spacing. Grooves were then selectively zinc metalized at 500 nm thickness. Grooves were examined with Keyence VHX, and a good agreement with previous results was found. Modified module #1 has two strips 182 × 4 mm each; modified module #2 has five strips 182 × 4 mm each. Figure 15 shows the arrangement of the modifications.

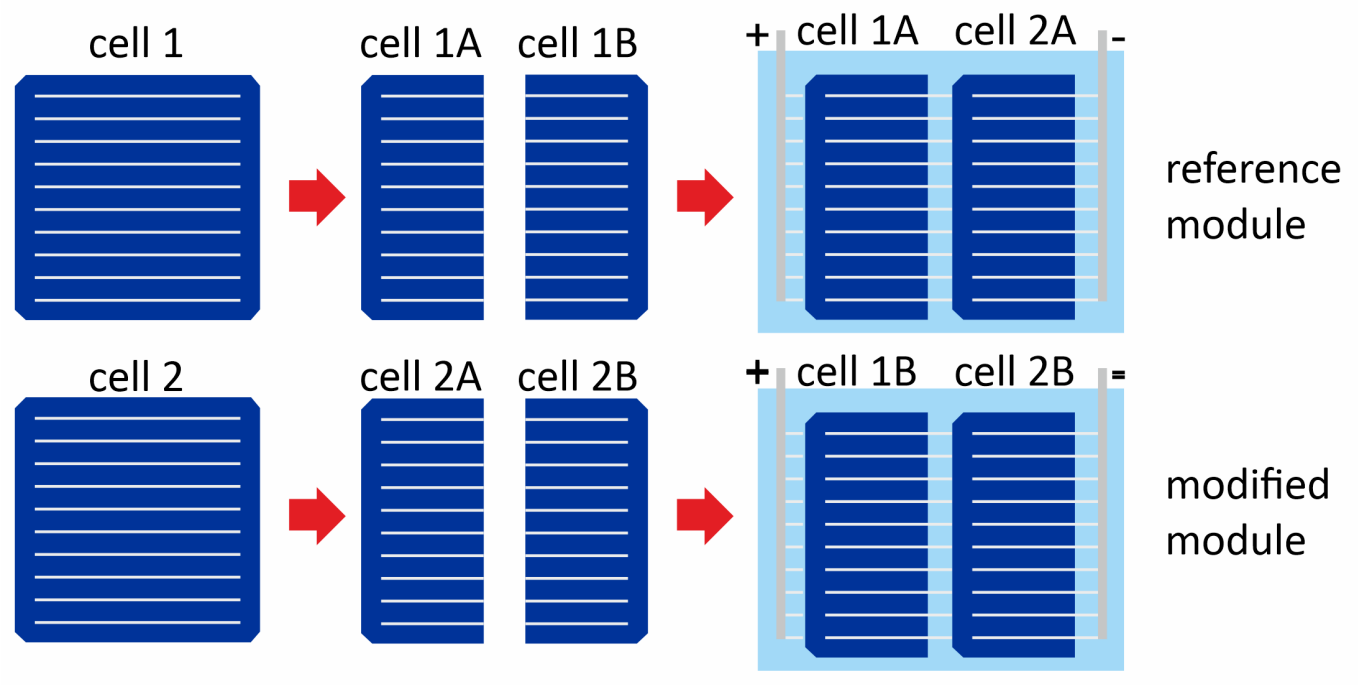


**Figure 14.** The self-compensating cell arrangement in minimodules for direct electrical comparison.

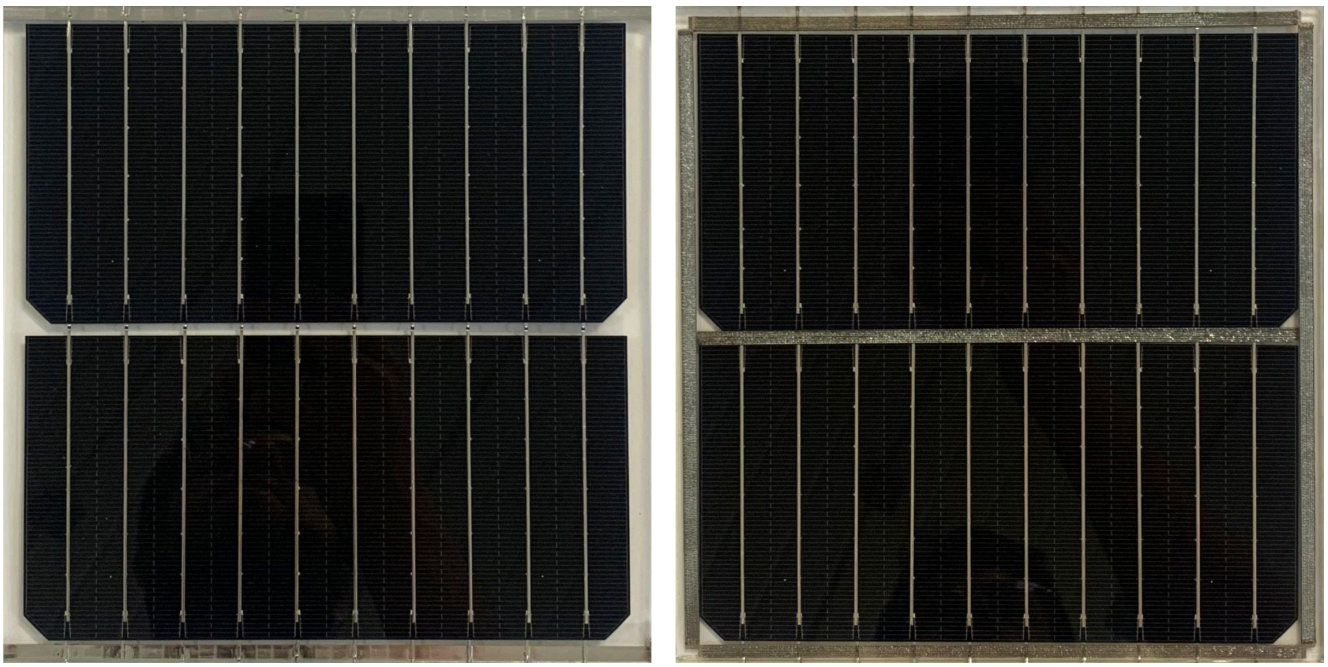

**Figure 15.** (**Left**)—modified module #1, (**right**)—modified module #2.

The modules were subject to an electroluminescence check, and no cracks or damage were detected in the samples. Figures 15 and 16 presents photographs of the reference and modified modules.

Modules produced in such a way were then tracked for current-voltage characteristics using a solar radiation simulator of AAA class, model SS200AAA EM by Photo Emission Tech., Inc., and a SS I-V CT-02 system with PV Test Solution software at an irradiance of 1000 W/m$^2$ and AM1.5 spectrum. The obtained results are listed in Table 1.

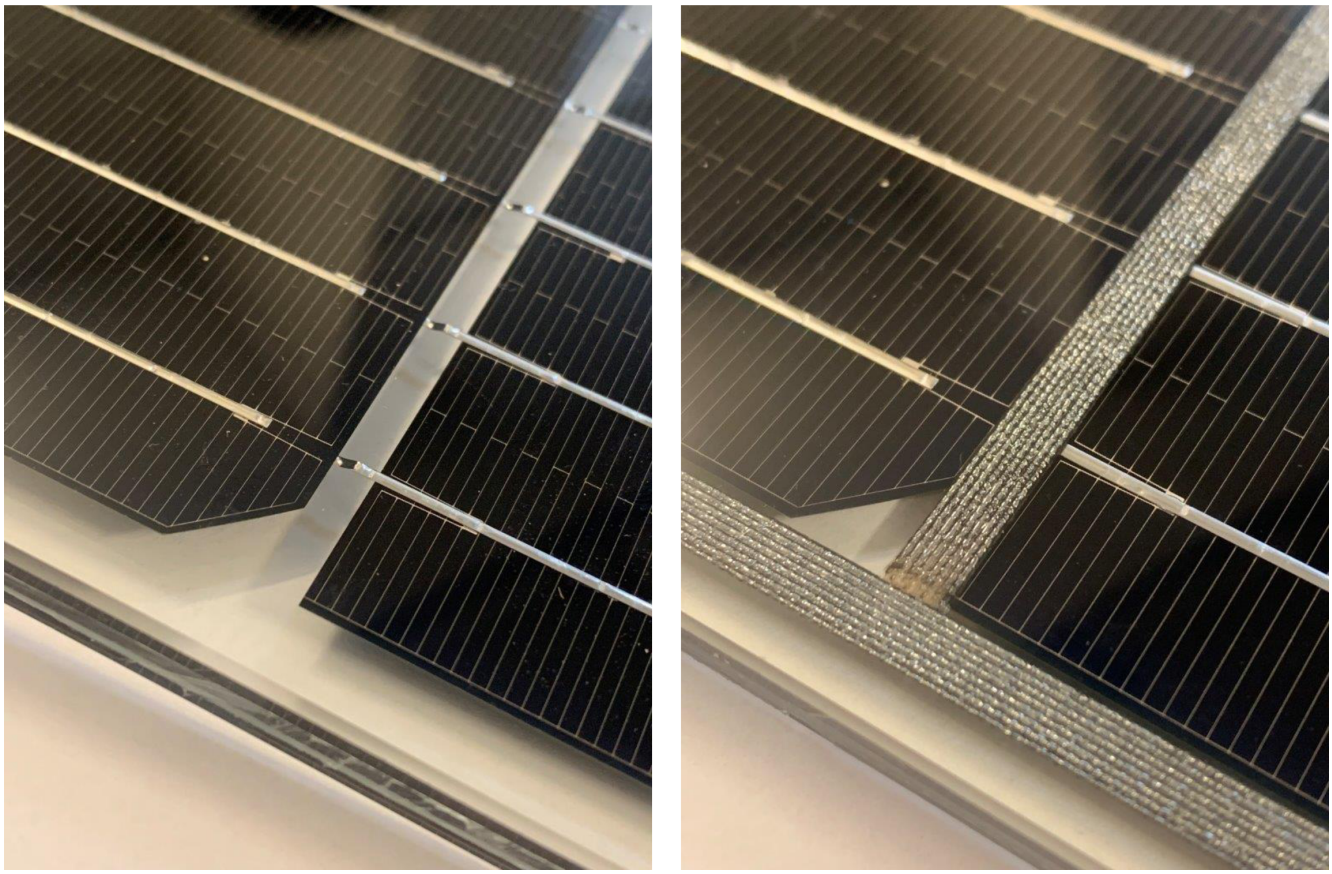

**Figure 16.** Photo of minimodules used for proof of concept. (**Left**)—reference, (**right**)—modified.

**Table 1.** I-V characteristics of minimodules prepared as a proof of concept.

| Measured Element | | Isc [mA] | Voc [mV] | Im [mA] | Vm [mV] | Pm [mW] | FF [-] | Eff [%] |
|---|---|---|---|---|---|---|---|---|
| Pair#1 | Reference module #1 | 5.668 | 1.3639 | 5.465 | 1.1594 | 6.336 | 0.82 | 15.84 |
| | Modified module #1 | 5.735 | 1.3641 | 5.511 | 1.1592 | 6.388 | 0.817 | 15.97 |
| Pair#2 | Reference module #2 | 5.797 | 1.3661 | 5.561 | 1.1616 | 6.459 | 0.816 | 16.15 |
| | Modified module #2 | 5.885 | 1.3665 | 5.653 | 1.1606 | 6.561 | 0.816 | 16.4 |
| | Pair #1 CTM gain | 0.0670 | 0.0002 | 0.0460 | −0.0002 | 0.0520 | −0.0030 | 0.1300 |
| | Pair #2 CTM gain | 0.088 | 0.000 | 0.092 | −0.001 | 0.102 | 0.000 | 0.250 |
| | Pair #1 CTM relative gain | 1.18% | 0.01% | 0.84% | −0.02% | 0.82% | −0.37% | 0.82% |
| | Pair #2 CTM relative gain | 1.52% | 0.03% | 1.65% | −0.09% | 1.58% | 0.00% | 1.55% |

Modified module #1 has a total area of 1456 $mm^2$ of modifications, which are 4.4% of the active cells used in the module. Modified module #2 has a total area of 3640 $mm^2$ of modifications, which accounts for 11% of the active solar cell area. Because of the small size of the module, the modifications are not symmetrical, and work as marginal. From the symmetry, it can be assumed that marginal modification works at 50% efficiency.

The results clearly show a positive effect on the CTM power ratio. The achieved CTM power gain is 1.58%, and this can be further improved in the standard scale module. This measurement result can be considered to be a proof of concept for the proposed solution.

## 4. Conclusions

A typical photovoltaic (PV) module has a significant part of 7–8% of the surface, which is left uncovered by silicone cells due to technological constraints. A sawtooth-shaped reflecting diffusor placed between solar cells is proposed as a way to increase the PV module

CTM ratio. The ray tracing simulation shows that the optimum pitch angle to achieve is from 122° to 132°. An important finding is that it is also possible to achieve zero percent efficiency; therefore, certain angles are to be avoided. The CW mode $CO_2$ laser interacting with soda-lime glass can process desired and uniform shapes and sizes of grooves in the glass. However, this is only possible under stable conditions when the air flow for focusing optics protection is not affecting the heating zone. The desired "V"-shaped grooves are achieved in the range of laser power of 20–30 W and a scan speed of 80–140 mm/s with a short focal length. Longer focal lengths lead to more "U" shaped profiles. The optimum parameters were found to be: F = 50.8 mm, P = 25 W, and V = 75 mm/s; and they were chosen to make minimodules for the proof of concept. Solar simulator I-V measurement results clearly show a positive effect on the CTM ratio. The achieved power gain was 1.58%, and this can be further optimized in standard scale modules. Changes in the mechanical parameters of glass are to be further studied, and their influence on PV module mechanical performance is to be evaluated. The influence on the module lamination process is to be investigated further to prove that the proposed modification has no negative impact on module durability. A strong advantage of the proposed solution is high selectivity and precision on large surfaces of photovoltaic modules, which, together with the high speed and energetic efficiency of the process, create the possibility of incorporating such modifications into the regular, existing manufacturing process of photovoltaic modules, including and beyond silicon technology. This modification can be applied in intercell areas, margins, and above ribbons as well. The proposed solution is mainly dedicated to high-performance bifacial modules. The laser-based selective metallization process is developed by the authors in parallel, which can be a good match to the solution proposed here.

**Author Contributions:** Conceptualization, O.J. and K.D.; data curation, O.J. and P.S.; formal analysis, W.F.; funding acquisition, O.J. and K.D.; investigation, O.J., P.N., F.S., P.S., P.K. and K.D.; methodology, O.J. and K.D.; project administration, K.D.; resources O.J. and P.S.; supervision, K.D.; validation, G.K.-M. and W.F.; visualization, P.S.; writing—original draft, O.J.; writing—review and editing, P.K., W.F. and K.D. All authors have read and agreed to the published version of the manuscript.

**Funding:** This work is a part of the Ph.D. study, "Laminating processes of photovoltaic (PV) modules based on materials modified by laser surface treatment techniques", carried out as part of the "Implementation Doctorate" program of the Ministry of Education and Science in Poland project No DWD/4/42/2020.

**Institutional Review Board Statement:** Not applicable.

**Informed Consent Statement:** Not applicable.

**Data Availability Statement:** Not applicable.

**Conflicts of Interest:** The authors declare no conflict of interest.

## References

1. Ajayan, J.; Nirmal, D.; Mohankumar, P.; Saravanan, M.; Jagadesh, M.; Arivazhagan, L. A review of photovoltaic performance of organic/inorganic solar cells for future renewable and sustainable energy technologies. *Superlattices Microstruct.* **2020**, *143*, 106549. [CrossRef]
2. International Technology Roadmap for Photovoltaic (ITRPV) 13th Edition, Published by the German Mechanical Engineering Industry Association (VDMA). March 2022. Available online: https://www.vdma.org/international-technology-roadmap-photovoltaic (accessed on 12 August 2022).
3. Su, W.-S.; Chen, Y.-C.; Liao, W.H.; Huang, C.-H.; Liu, D.-C.; Huang, M.-Y.; Wu, Z.-C.; Ho, S.-J. Optimization of the output power by effect of backsheet reflectance and spacing between cell strings. In Proceedings of the 37th IEEE Photovoltaic Specialists Conference, Seattle, WA, USA, 19–24 June 2011; pp. 3218–3220. [CrossRef]
4. Lim, H.; Cho, S.H.; Moon, J.; Jun, D.Y.; Kim, S.H. Effects of Reflectance of Backsheets and Spacing between Cells on Photovoltaic Modules. *Appl. Sci.* **2022**, *12*, 443. [CrossRef]
5. McIntosh, K.R.; Jung, J.; Abbott, M.D.; Sudbury, B.A. Determination and evaluation of a backsheet's intrinsic reflectance. In Proceedings of the AIP Conference Proceedings, Lausanne, Switzerland, 19–21 March 2018; AIP Publishing LLC: Melville, NY, USA, 2018; Volume 1999, p. 020018. [CrossRef]

6. Mittag, M.; Grünzweig, A.; Wiese, M.; Mahmoud, N.; Schmid, A.; Heinrich, M. Analysis of backsheet and rear cover reflection gains for bifacial solar cells. In Proceedings of the 33rd European PV Solar Energy Conference and Exhibition (Vol. 2017), Amsterdam, The Netherlands, 25–29 September 2017.
7. Sarniak, M.T. Modeling the Functioning of the Half-Cells Photovoltaic Module under Partial Shading in the Matlab Package. *Appl. Sci.* **2020**, *10*, 2575. [CrossRef]
8. Jang, J.; Pfreundt, A.; Mittag, M.; Lee, K. Performance Analysis of Bifacial PV Modules with Transparent Mesh Backsheet. *Energies* **2021**, *14*, 1399. [CrossRef]
9. Hanifi, H.; Dassler, D.; Schneider, J.; Turek, M.; Schindler, S.; Bagdahn, J. Optimized tab width in half-cell modules. *Energy Procedia* **2016**, *92*, 52–59. [CrossRef]
10. Bae, J.; Jee, H.; Park, Y.; Lee, J. Simulation-Based Shading Loss Analysis of a Shingled String for High-Density Photovoltaic Modules. *Appl. Sci.* **2021**, *11*, 11257. [CrossRef]
11. Shin, G.; Jeon, J.G.; Kim, J.H.; Lee, J.H.; Kim, H.J.; Lee, J.; Kang, K.M.; Kang, T.J. Thermocells for Hybrid Photovoltaic/Thermal Systems. *Molecules* **2020**, *25*, 1928. [CrossRef]
12. Haedrich, I.; Eitner, U.; Wiese, M.; Wirth, H. Unified methodology for determining CTM ratios: Systematic prediction of module power. *Sol. Energy Mater. Sol. Cells* **2014**, *131*, 14–23. [CrossRef]
13. Yousuf, H.; Zahid, M.A.; Khokhar, M.Q.; Park, J.; Ju, M.; Lim, D.; Kim, Y.; Cho, E.-C.; Yi, J. Cell-to-Module Simulation Analysis for Optimizing the Efficiency and Power of the Photovoltaic Module. *Energies* **2022**, *15*, 1176. [CrossRef]
14. Haedrich, I.; Surve, S.; Thomson, A. Cell to module (CTM) ratios for varying industrial cell types. In Proceedings of the 2015 Asia Pacific Solar Research Conference, Melbourne, Australia, 8–10 December 2015; pp. 1–6.
15. Mariano, J.R.L.; Lin, Y.-C.; Liao, M.; Ay, H. Analysis of Power Generation for Solar Photovoltaic Module with Various Internal Cell Spacing. *Sustainability* **2021**, *13*, 6364. [CrossRef]
16. Sharma, A.; Dasgotra, A.; Tiwari, S.K.; Sharma, A.; Jately, V.; Azzopardi, B. Parameter Extraction of Photovoltaic Module Using Tunicate Swarm Algorithm. *Electronics* **2021**, *10*, 878. [CrossRef]
17. Sanchez-Illescasa, P.J.; Carpena, P.; Bernaola-Galva, P.; Sidrach-de-Cardona, M.; Coronado, A.V.; Alvarez, J.L. An analysis of geometrical shapes for PV module glass encapsulation. *Sol. Energy Mater. Sol. Cells* **2008**, *92*, 323–331. [CrossRef]
18. Blieske, U.; Doege, T.; Gayout, P.; Neander, M.; Neumann, D.; Prat, A. Light-trapping in solar modules using extra-white textured glass. In Proceedings of the 3rd World Conference on Photovoltaic Energy Conversion, Osaka, Japan, 11–18 May 2003; Volume 1, pp. 188–191. Available online: https://ieeexplore.ieee.org/abstract/document/1305253 (accessed on 12 August 2022).
19. McIntosh, K.R.; Swanson, R.M.; Cotter, J.E. A simple ray tracer to compute the optical concentration of photovoltaic modules. *Prog. Photovolt. Res. Appl.* **2006**, *14*, 167–177. [CrossRef]
20. Yang, G.; van Swaaij, R.A.; Isabella, O.; Zeman, M. A novel way of texturing glass for microcrystalline silicon thin film solar cells application. *Prog. Photovolt. Res. Appl.* **2015**, *23*, 1283–1290. [CrossRef]
21. Hussain, S.Q.; Le, A.H.T.; Mallem, K.; Park, H.; Ju, M.; Cho, J.; Park, J.; Cho, E.; Cho, Y.H.; Kim, Y.; et al. Advanced Light scattering through various textured glass surface morphologies in thin film silicon solar cells. In Proceedings of the 2018 IEEE 7th World Conference on Photovoltaic Energy Conversion (WCPEC) (A Joint Conference of 45th IEEE PVSC, 28th PVSEC & 34th EU PVSEC), Waikoloa, HI, USA, 10–15 June 2018; pp. 3090–3096. [CrossRef]
22. Das, S.; Kundu, A.; Banerjee, C.; Dey, P.; Datta, S.K.; Saha, H. *Front Surface Glass Texturization for Improved Performance of Amorphous Silicon Solar Cell*; Springer: Cham, Switzerland, 2014; pp. 375–378. [CrossRef]
23. Kim, M.S.; Lee, J.H.; Kwak, M.K. Surface texturing methods for solar cell efficiency enhancement. *Int. J. Precis. Eng. Manuf.* **2020**, *21*, 1389–1398. [CrossRef]
24. Peters, M.; Bielawny, A.; Bläsi, B.; Carius, R.; Glunz, S.W.; Goldschmidt, J.C.; Hauser, H.; Hermle, M.; Kirchartz, T.; Löper, P.; et al. Photonic concepts for solar cell. In *Physics of Nanostructured Solar Cells*; Badescu, V., Paulescu, M., Eds.; Nova Science Publishers: Hauppauge, NY, USA, 2010; pp. 1–41. ISBN 978-1-60876-110-4.
25. Alqurashi, T.; Alhosani, A.; Dauleh, M.; Yetisen, A.; Butt, H. Laser inscription of pseudorandom structures for microphotonic diffuser applications. *Nanoscale* **2018**, *10*, 7095–7107. [CrossRef]
26. Homma, H.; Kagotani, A.; Moronaga, K.; Murillo-Mora, L.M. Solar Battery Module. US Patent Publication US2011/0186114 A1, 4 August 2011. Available online: https://worldwide.espacenet.com/patent/search?q=pn%3DUS2011186114A1 (accessed on 7 July 2022).
27. O'Neill, M.; Ma, J.; Votava, M. Light Redirecting Film Useful with Solar Modules. International Application Published under Patent Cooperation Treaty (PCT) WO2016168164A1, 20 October 2016. Available online: https://worldwide.espacenet.com/patent/search?q=pn%3DWO2016168164A1 (accessed on 7 July 2022).
28. Kang, S.; Shin, J. Experimental investigation on the $CO_2$ laser cutting of soda-lime glass. *J. Mech. Sci. Technol.* **2020**, *34*, 3345–3351. [CrossRef]
29. Brusberg, L.; Queisser, M.; Gentsch, C.; Schröder, H.; Lang, K.D. Advances in $CO_2$-Laser Drilling of Glass Substrates. *Phys. Procedia* **2012**, *39*, 548–555. [CrossRef]
30. Zhimalov, A.B.; Solinov, V.F.; Kondratenko, V.S.; Kaplina, T.V. Laser cutting of float glass during production. *Glass Ceram.* **2006**, *63*, 9–10. [CrossRef]

31. Sindhu, I.; Rahman, R.A. Formation of microgrooves on glass and PMMA using low power $CO_2$ laser. *J. Optoelectron. Adv. Mater.* **2012**, *14*, 877–884.
32. Allcock, A.; Dyer, P.E.; Elliner, G.; Snelling, H.V. Experimental observations and analysis of $CO_2$ laser-induced microcracking of glass. *J. Appl. Phys.* **1995**, *78*, 7295–7303. [CrossRef]
33. Lax, M. Temperature rise induced by a laser beam. *J. Appl. Phys.* **1977**, *48*, 3919. [CrossRef]